ACS OMEGA

Open Access

http://pubs.acs.org/journal/acsodf

Article

Solvent-Free Synthesis of Fumarate-Based Metal−Organic Frameworks with Resonant Acoustic Mixing

Laura I. FitzGerald, Ashley L. Sutton, Aaron J. Seeber, Benjamin W. Muir, and Cara M. Doherty*

Cite This: *ACS Omega* 2025, 10, 19206−19213

Read Online

ACCESS | Metrics & More | Article Recommendations | Supporting Information

ABSTRACT: Metal-organic frameworks (MOFs) are versatile materials, but their synthesis often requires harsh conditions, toxic precursors, or organic solvents. Recently, MOFs have been produced using resonant acoustic mixing (RAM), a form of mechanochemistry that provides a greener alternative to conventional methods. In this study, we demonstrate the solvent-free synthesis of fumarate-based MOFs using RAM at room temperature and atmospheric pressure. Iron fumarate (MIL-88A(Fe)) was successfully produced with a BET surface area of 209 m^2 g^{-1}, comparable to mechanochemical grinding. The synthesis was scaled up to a 10.5 g yield using RAM for 20 min and without solvent. Aluminum fumarate (MIL-53(Al)-FA) was also synthesized with a high surface area (790 m^2 g^{-1}), while attempts to synthesize the calcium fumarate MOF (CaFu) instead resulted in the non-porous coordination polymer, calcium fumarate trihydrate. These results demonstrate the potential of RAM as a more sustainable approach to MOF synthesis.

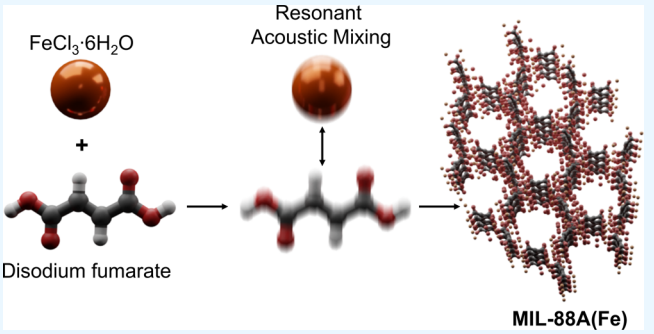

INTRODUCTION

Metal−organic frameworks (MOFs) are porous materials widely studied for their adsorption and molecular separations in environmental applications.[1] However, many synthesis routes rely on toxic solvents, high temperatures, or long reaction times, making them less sustainable.[2] Mechanochemistry, including ball milling and grinding, uses mechanical force to drive chemical reactions and can be a greener alternative for MOF synthesis, as it requires little to no solvent and shorter reaction times.[3,4]

Beyond synthesis conditions, the choice of metal nodes and linkers plays a key role in MOF environmental viability. Iron, aluminum, and calcium are considered lower-toxicity alternatives to zinc, copper, and manganese,[5] while fumaric acid, a biologically occurring molecule,[6] is among the most biodegradable and environmentally benign linkers.[5] These components form MIL-88A(Fe),[7] MIL-53(Al)-FA (BASF A520),[8,9] and CaFu[10,11]—MOFs with potential for water purification[10,12−15] and gas capture.[16] MIL-88A(Fe) has previously been synthesized by manual grinding[17] and aluminum fumarate by twin-screw extrusion.[18] However, only limited reports on CaFu exist, and no mechanochemical route has been described.

Recently, Resonant Acoustic Mixing (RAM) has been reported as a novel mechanochemical approach for MOF synthesis, allowing solvent-free production under ambient conditions.[19] Zinc-based MOFs such as ZIF-8 and ZIF-L, as well as the copper-based HKUST-1, were synthesized in as little as 5 min and scaled up to 25 g. RAM uses acoustic waves to efficiently blend powders,[20] offering improved reproducibility over manual grinding and eliminating solvent waste. In this example, a small amount of solvent was added (0.3 μL per mg of dry starting material). This places the reaction in the category of liquid-assisted grinding (LAG), which is defined by a liquid-to-solid ratio (η) between 0 and 1 μL mg^{-1}.[21] In contrast, neat grinding corresponds to $\eta = 0$, while solution synthesis typically involves $\eta > 10$ μL mg^{-1}.[21] Unlike twin-screw extrusion, reactions occur in closed vessels, reducing exposure risks and direct contact with equipment.[22] Since RAM operates at room temperature and atmospheric pressure, it may offer significant energy savings over solvothermal methods, which typically require temperatures of 50−260°C and long reaction times.[23]

In this study, we demonstrate the solvent-free synthesis of low-toxicity fumarate-based MOFs by RAM as a step toward their greener production (Figure 1). We show that MIL-88A(Fe) can be synthesized rapidly and scaled up efficiently, while RAM also enables the synthesis of MIL-53(Al)-FA. Although CaFu did not form as a MOF phase under these conditions, these results highlight RAM's potential for

Received: March 11, 2025
Revised: April 6, 2025
Accepted: April 14, 2025
Published: April 29, 2025

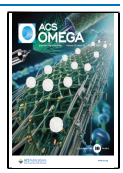

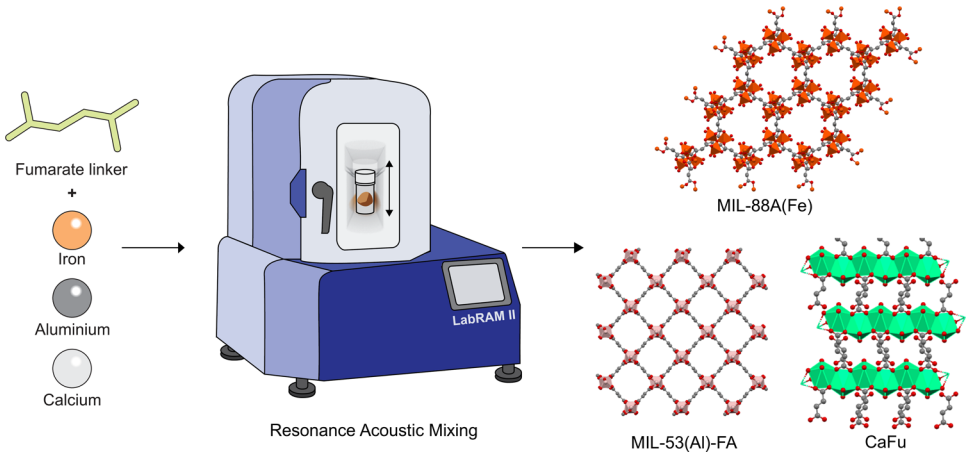

Figure 1. Synthesis of fumarate-based MOFs using RAM with the LabRAM II by Resodyn.

sustainable MOF synthesis, particularly for environmentally relevant adsorbents.

RESULTS AND DISCUSSION

Initial attempts at producing MIL-88A(Fe) by RAM were adapted from the prior mechanochemical synthesis by manual grinding. In that report, equimolar amounts of iron(III) chloride hexahydrate and disodium fumarate were ground in a mortar and pestle, followed by washing with water then acetone.[17] While fumaric acid is typically used in MIL-88A(Fe) synthesis, disodium fumarate improves deprotonation and solubility at room temperature in the presence of water, aiding formation.[24]

We combined these same amounts of iron(III) chloride hexahydrate and disodium fumarate in 20 mL plastic vials and subjected them to RAM. Acceleration (measured in m s^{-2} or *g*) and reaction time were varied—the two adjustable parameters on the RAM instrument. Conditions included a constant mixing time of 60 min at 45, 60, and 75*g* and a constant acceleration of 75*g* for 20 and 40 min. These were chosen based on the prior MOF RAM study[19] where acceleration below 45*g* resulted in incomplete conversion. Unlike that report, we performed neat grinding (η = 0) by omitting the small amount of liquid (0.3 μL mg^{-1}) they added, anticipating that the hydration of the metal salt would provide sufficient water for the reaction. Products were washed in water then acetone and air dried.[17] As a control, we also synthesized MIL-88A(Fe) in water at 60°C for 4 h without RAM following a previously described method.[17]

The samples were characterized using powder X-ray diffraction (PXRD). All samples, except for the 75*g*, 60 min sample matched the literature diffractogram[25] and the simulated pattern for MIL-88A(Fe) (Figure 2a). However, an additional peak at ∼12° 2θ was present, along with broadening or splitting of the peak at 10° 2θ, forming an additional reflection at ∼10.8° 2θ. These arise from the coexistence of open and closed forms of MIL-88A(Fe) due to the reversible framework swelling.[26] By preparing a slurry in water, the fully wet sample matched the simulated open phase, with the additional reflections disappearing upon hydration (Figure S1). While our experimental setup does not allow us to confirm whether the framework fully closes upon activation, this should be investigated further in future studies.

Fourier Transform Infrared Spectroscopy (FTIR) was used to characterize functional groups and bonding in the samples.

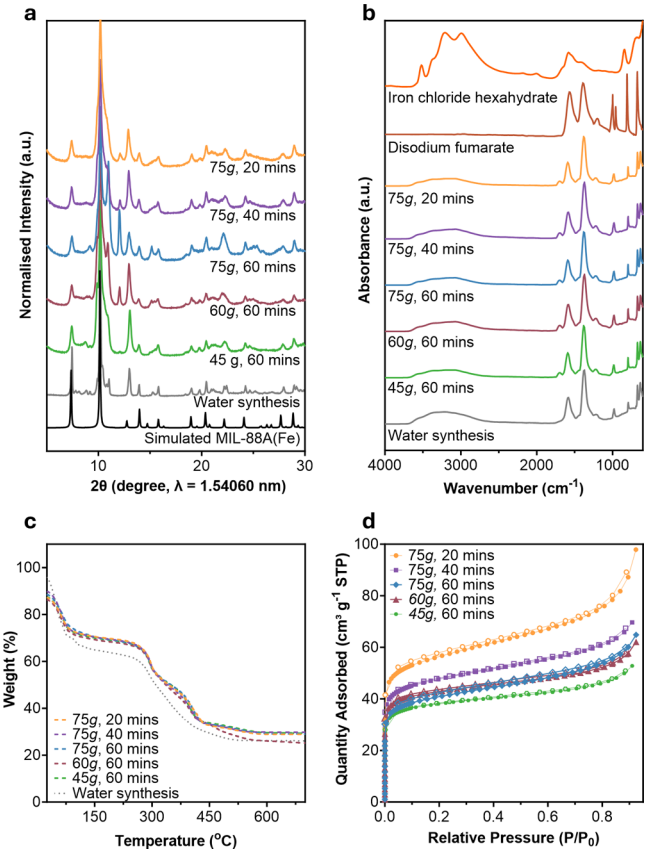

Figure 2. Characterization of MIL-88A(Fe) synthesized under constant time or acceleration compared to water synthesis. (a) PXRD patterns, (b) FTIR spectra, (c) TGA profiles, and (d) nitrogen sorption analysis (symbols: closed = adsorption, open = desorption).

The spectra of all samples were similar regardless of reaction time or acceleration (Figure 2b and Table S1), matched the control MIL-88A(Fe) sample synthesized in water, and were also similar to disodium fumarate, as expected for carboxylate salt-based MOFs.[27] Approximate peak assignments include: 1380 and 1588 cm^{-1} as symmetric and asymmetric vibrations of the carboxyl group of fumarate, 981 cm^{-1} as out-of-plane carbon to hydrogen bending and 1217 cm^{-1} as stretching of carbon to oxygen.[27,28] A broad band above 3000 cm^{-1}

https://doi.org/10.1021/acsomega.5c02296
ACS Omega 2025, 10, 19206−19213

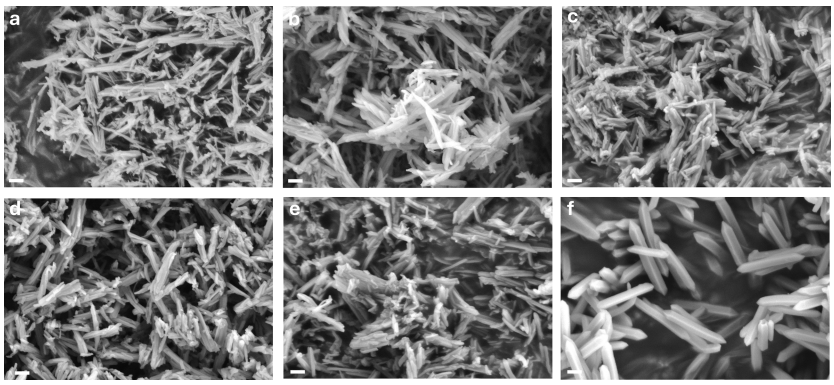

Figure 3. SEM images at 30k magnification of MIL-88A(Fe) samples synthesized by RAM at (a) 75*g*, 20 min, (b) 75*g*, 40 min, (c) 75*g*, 60 min, (d) 60*g*, 60 min, (e) 45*g*, 60 min, or (f) without RAM in water. Scale bar = 200 nm.

corresponds to residual water in the structure, absent in disodium fumarate (Figure 2b).

Thermogravimetric analysis (TGA) was performed to assess thermal stability and composition changes upon heating. TGA plots were nearly identical across all samples and matched literature reports and the control MIL-88A(Fe) sample (Figure 2c). An initial ∼20% mass loss (25−190°C) corresponds to water loss, followed by a second decrease at 340°C due to fumaric acid decomposition and framework collapse (Figure 2c).[29,30] To identify defects, the theoretical residual mass-to-total mass ratio was compared to experimental TGA values.[31] Ligand defects ranged from 3 to 20% across all samples, with no clear correlation to reaction time or applied acceleration (Table S2).

Porosity was evaluated using nitrogen adsorption via Brunauer−Emmett−Teller (BET) surface area analysis (Figure 2d). BET surface areas ranged from 143−209 $m^2\ g^{-1}$ (Table S3), exceeding the 108 $m^2\ g^{-1}$ reported for MIL-88A(Fe) synthesized by grinding[17] and significantly exceeding some solution-based methods (∼6−30 $m^2\ g^{-1}$).[13,32] All RAM-synthesized samples, except the 45*g*, 60 min sample (143 $m^2\ g^{-1}$) exceeded the control MIL-88A(Fe) (149 $m^2\ g^{-1}$). This difference in BET surface area (143−209 $m^2\ g^{-1}$ vs literature values of 6−30 $m^2\ g^{-1}$ for solution-based synthesis) could indicate incomplete closure of the framework following activation.

Pore size distribution analysis revealed a sharp peak at approximately 5.3 Å (Figure S2), consistent with the theoretical ∼6.6 Å pore width estimated from crystallographic data.[25] These results indicate predominantly microporous material with minor mesoporosity, likely from interparticle voids. *t*-plot analysis (Table S4) supports this, showing that the 75*g*, 20 min sample had the highest BET surface area (209 $m^2\ g^{-1}$) and largest external surface area (80.5 $m^2\ g^{-1}$). The trend follows across the series and may be influenced by smaller and/or less uniform particles at reduced mixing times.

Scanning electron microscopy (SEM) revealed that MIL-88A(Fe) synthesized by RAM predominantly formed rod-like structures (Figure 3), a typical morphology of this MOF.[33] However, the rods appeared deformed compared to those synthesized in water (Figure 3f), likely due to mechanical effects.[34] Energy Dispersive X-ray Spectroscopy (EDXS) confirmed the expected presence of carbon and oxygen from the fumarate linker, along with iron from the metal node (Figure 4). Collectively, these results demonstrate the robust formation of MIL-88A(Fe), showing that its structure is relatively independent of reaction time and acceleration.

RAM is highly scalable, typically in pursuit of larger yields. However, to simplify screening for the synthesis of other MOFs, we aimed to scale down the process. Smaller precursor amounts in the same vial may not mix optimally, so using a custom 3D-printed holder (Figure S3), we attempted MIL-88A(Fe) synthesis with 1/7th the starting material (∼0.6 g total) in 1.5 mL tubes. After 60 min at 45*g*, followed by washing with the same solvents as before, PXRD confirmed a match with the simulated MIL-88A(Fe) phase (Figure S4). This 7-fold downscaling aligns with previous reports of RAM scalability.[19]

We also scaled up the process, subjecting 13.5 g of iron(III) chloride and 8 g of disodium fumarate to RAM at 75*g* for 20 min in a 100 mL polypropylene autoclave liner. This again yielded MIL-88A(Fe), confirmed by PXRD (Figure S4). The yield (10.5 g) was 8-fold higher than that obtained with 5-fold lower precursor amounts (1.3 g), likely due to improved mixing efficiency related to vessel geometry rather than changes in stoichiometry.[35] At this scale, the BET surface area reached 248.1 $m^2\ g^{-1}$ (Figure S5), 1.3 times higher than at lower scales, with an external surface area of 68.9 $m^2\ g^{-1}$ (Table S5). The intense peak at ∼6 Å in the pore size distribution again aligns with the theoretical pore width of the open framework (Figure S6).[26] Collectively, these results demonstrate the scalability and reproducibility of RAM, highlighting its adaptability across different synthesis scales.

To demonstrate the versatility of the method, we attempted to produce two related MOFs, MIL-53(Al)-FA and CaFu. The industrial synthesis of aluminum-based MIL-53(Al)-FA is conducted at ambient pressure and 60°C for 4 h, using aluminum sulfate octadecahydrate, water as the solvent and sodium hydroxide to aid in solubilising the fumaric acid linker.[8,9] For synthesis by RAM, we kept the ratio of ligand to metal the same (2:1) and included a small amount of sodium hydroxide (0.13 $\mu L\ mg^{-1}$). This was not intended for solubilising the linker or assisting with grinding, as in the previous RAM synthesis of MOFs (where 0.3 $\mu L\ mg^{-1}$ was used).[19] Instead it was used due to the internal structure of MIL-53(Al)-FA, which features a bridging hydroxyl group between aluminum nodes.[9]

In contrast, the synthesis of the porous CaFu MOF has not been as thoroughly investigated as MIL-53(Al)-FA.[10,11] The more facile synthesis of the existing reports combines fumaric acid and calcium acetate at approximately 0.2 mM in water,

https://doi.org/10.1021/acsomega.5c02296
ACS Omega 2025, 10, 19206−19213

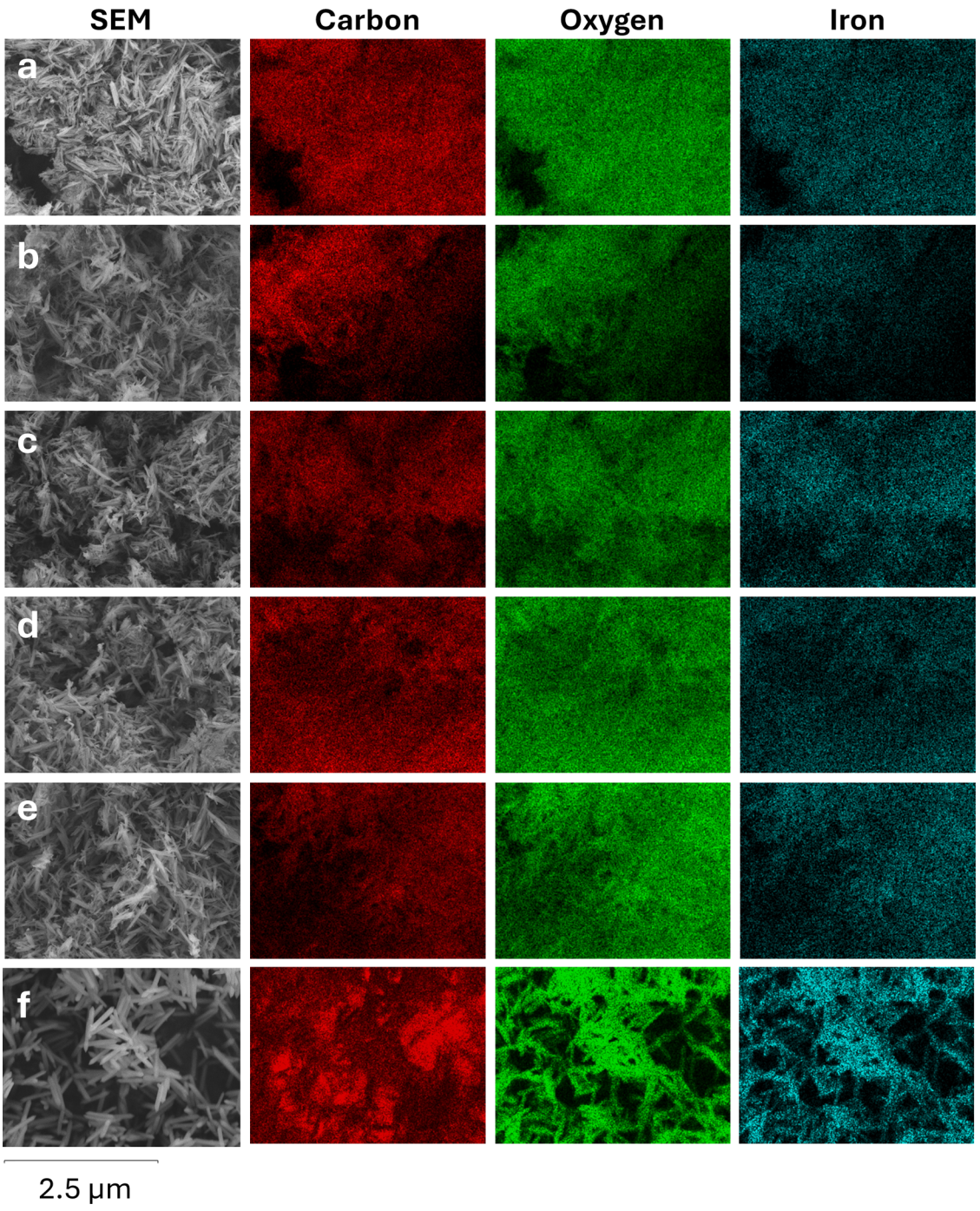

Figure 4. Elemental composition of MIL-88A(Fe) samples by EDXS synthesized by RAM at (a) 75*g*, 20 min, (b) 75*g*, 40 min, (c) 75*g*, 60 min, (d) 60*g*, 60 min, (e) 45*g*, 60 min, or (f) without RAM in water.

and requires autoclaving for 16 h at 65°C. We kept the ratio of solids the same and in this case, did not add any liquid. To maintain a similar scale to MIL-88A(Fe), the total mass of reactants was fixed at ∼0.5−0.6 g in the 1.5 mL vial. Samples were subjected to RAM for 60 min at an intermediate acceleration of 60*g*. Following mixing, the samples were sequentially washed with water and ethanol, then air-dried before characterization.

PXRD showed the aluminum RAM sample was a reasonable match to the simulated MIL-53(Al)-FA phase (Figure 6). Although poorly crystalline, this is typical of this MOF.[9] Synthesis was also attempted without any liquid additive. The PXRD pattern remained similar, indicating the formation of MIL-53(Al)-FA (Figure S7), but the yield drastically decreased from 114 mg to 47 mg. This suggests that some water from the metal salt (aluminum sulfate octadecahydrate) can provide the necessary −OH groups for bridge formation, but the reaction efficiency increases when additional hydroxide is supplied.

A previous report for the CaFu MOF showed it shares the same crystal structure as calcium fumarate hydrate with slightly smaller lattice parameters.[11] Comparison of this diffractogram with the calcium RAM sample demonstrated it was composed of well crystallized calcium fumarate along with minor unknown phases (Figure 5a). However, the calcium sample

https://doi.org/10.1021/acsomega.5c02296
ACS Omega 2025, 10, 19206−19213

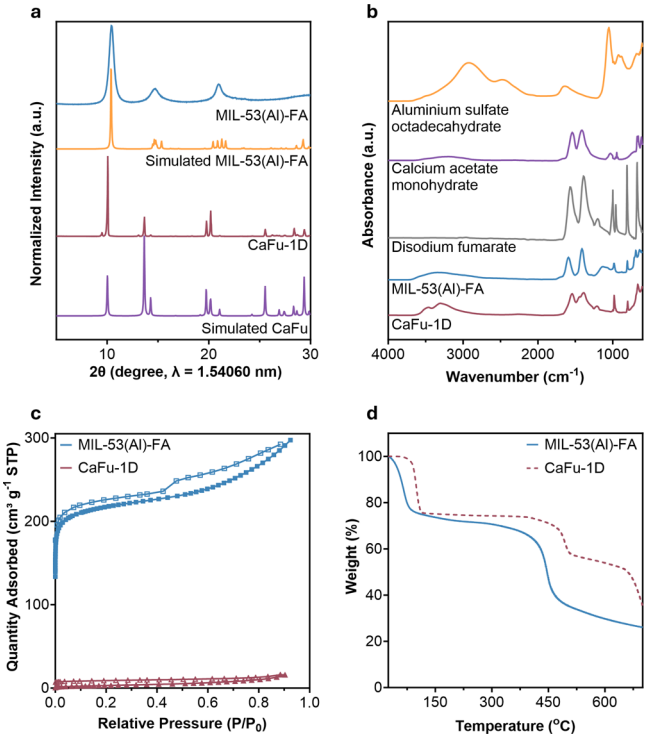

Figure 5. Characterization of MIL-53(Al)-FA and CaFu-1D by (a) PXRD, (b) FTIR, (c) BET surface area analysis (solid line = adsorption, dotted line = desorption), and (d) TGA synthesized by RAM at 60*g* for 60 min.

was non-porous with a BET surface area of 11.1 $m^2 g^{-1}$ (Figure 5c). A follow-up attempt at a higher acceleration (75*g*, 60 min) resulted in the same phase as determined by PXRD (Figure S8), but the material remained non-porous with a BET surface area of only 4 $m^2 g^{-1}$ (Figure S9). Since the CaFu MOF and calcium fumarate hydrate share the same space group ($Pna2_1$) it is likely this is the product formed in our synthesis.[36,37] For clarity, we refer to our product as CaFu-1D in figures and text, as calcium fumarate hydrate is a 1D coordination polymer,[37] while CaFu is reserved for the porous MOF reported in the literature.

This is further supported by TGA analysis (Figure 5d), which shows an initial mass loss of about 26% around 120°C, close to the theoretical loss of 27% for three water molecules from calcium fumarate trihydrate ($CaC_4H_2O_4{\cdot}3H_2O$). Published studies on the CaFu MOF did not include TGA in their characterization, and no data could be found for calcium fumarate trihydrate. However, the shape and temperature values of our curve closely matched the decomposition of calcium oxalate monohydrate which occurs in three steps.[38] The first step is due to loss of water or acetone remaining in the pores. A second mass loss of 21% from 250 to 600°C was seen, which corresponds with formation of calcium carbonate. In the final step, a drop in mass of 18% was observed between 600 and 700°C due to further decomposition into calcium oxide.

The FTIR spectra for samples MIL-53(Al)-FA and CaFu were similar to that of MIL-88A(Fe) and shared many of the same peak assignments (Figure 5b and Table S6). The slight shifts in peak position for MIL-53(Al)-FA matched literature reports.[39,40] Additional peaks in the spectrum for CaFu-1D are attributed to hydroxyl stretching at 3734 cm^{-1}, carboxyl stretching at 3308 cm^{-1} and Ca−O vibration at 664 cm^{-1}.[10,11]

The BET surface area for the aluminum sample was 790 $m^2 g^{-1}$ (Figure 5c). Literature reports for MIL-53(Al)-FA[9,41] have values in the range of ∼808−1080 $m^2 g^{-1}$ which is in a similar range to our synthesis. An increased acceleration of 75*g* for 60 min did not significantly alter the PXRD pattern (Figure S8) and resulted in a slightly lower BET surface area of 714 $m^2 g^{-1}$ (Figure S9). TGA analysis showed MIL-53(Al)-FA decomposing in two steps at ∼70°C with a loss of 28% due to solvent evaporation and 430°C with a reduction of 46% from framework collapse due to degradation of fumarate (Figure 5d), comparable to previous studies.[42,43] Defect analysis indicated that approximately 9% of aluminum metal centres are missing.

SEM analysis revealed distinct morphologies between the samples. The MIL-53(Al)-FA sample consists of large agglomerations with a rough topology (Figure 6a), like

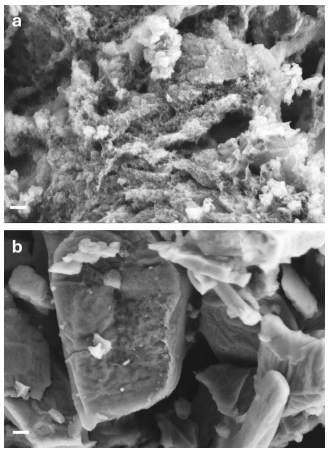

Figure 6. SEM images at 30k magnification of (a) MIL-53(Al)-FA and (b) CaFu-1D synthesized by RAM at 75*g* for 60 min. Scale bar = 200 nm.

industrially produced aluminum fumarate (BASF A520).[9] In contrast, the CaFu-1D sample possessed a more compact structure, forming solid blocks (Figure 6b). This differs significantly from reported SEM images of calcium fumarate MOFs, which typically show rougher surfaces with clear gaps.[10,11] This discrepancy supports the identification of our product as the coordination polymer rather than a 3D porous structure. EDXS analysis confirmed the presence of the expected elements: carbon and oxygen from the fumarate linker, along with aluminum for MIL-53(Al)-FA (Figure 7a) and calcium for calcium fumarate trihydrate (Figure 7b).

Finally, a preliminary estimation of RAM power consumption as a function of acceleration was conducted using an energy monitoring plug (Figure S10). Based on this relationship, the total energy requirement for the 75*g*, 20 min RAM synthesis of MIL-88A(Fe), using 2.7 g of iron(III) chloride and 1.6 g of disodium fumarate in a 7 g vial, was approximately 92 kJ. In contrast, a water-based synthesis over 4 h consumed an estimated 1057 kJ. Comparing the two methods shows that, for the same amount of starting material, RAM is approximately 11.5 times more energy-efficient than conventional laboratory oven synthesis. RAM also produced a higher yield (1.3 vs 0.48 g), further demonstrating its efficiency. Additionally, while water was used as the solvent

https://doi.org/10.1021/acsomega.5c02296
ACS Omega 2025, 10, 19206−19213

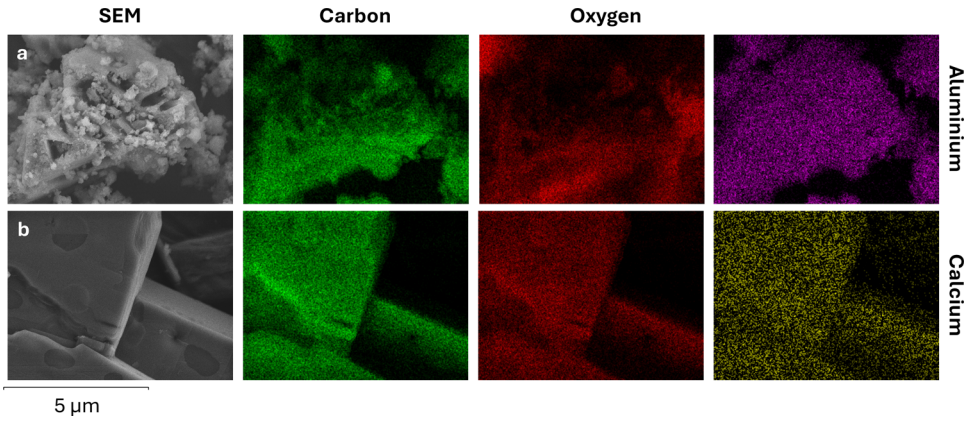

Figure 7. Elemental composition of (a) MIL-53(Al) and (b) CaFu-1D by EDXS.

here, RAM could provide even greater sustainability benefits when applied to MOFs typically synthesized in toxic solvents, by enabling solvent-free synthesis.

CONCLUSIONS

This study establishes RAM as a scalable, energy-efficient, and environmentally friendly method for synthesizing fumarate-based MOFs. We demonstrate, for the first time, the solvent-free, room-temperature, and atmospheric-pressure synthesis of MIL-88A(Fe) and MIL-53(Al)-FA via RAM. However, CaFu did not form under these conditions, instead yielding the coordination polymer calcium fumarate trihydrate (CaFu-1D). Beyond eliminating solvent use, RAM significantly reduced energy consumption compared to conventional synthesis, while maintaining high yields and surface areas. The method proved scalable, achieving a 10.5 g yield in 20 min, and has the potential for even larger-scale applications given that systems like the Resodyn RAM 55 accommodate up to 420 kg. While this work focused on fumarate-based MOFs, the addition of MIL-88A(Fe) and MIL-53(Al)-FA to those previously synthesized by RAM (ZIF-8, ZIF-L, and HKUST-1)[19] brings the total to five distinct frameworks, supporting RAM's broader applicability. Future work will focus on further upscaling and expanding RAM to other MOFs, particularly those sensitive to degradation in solution, as well as exploring its potential for biomolecule encapsulation. Although hydrated metal salts were used, no liquid was added, and the reactions fall under neat grinding conditions. The contribution of crystalline water to reaction outcomes remains an open question and may be explored in future work. This study highlights RAM's potential as a sustainable alternative for MOF synthesis, supporting broader efforts toward greener material production.

METHODS

MIL-88A(Fe) Water Synthesis. MIL-88 was synthesized in water as described previously.[17] Iron(III) chloride hexahydrate (2.7 g, 10 mmol) and disodium fumarate (1.6 g, 10 mmol), both dissolved separately in 50 mL water were combined in a 500 mL Schott Duran bottle and heated to 60°C in a synthesis oven for 4 h. The precipitate was washed once with 50 mL of water, once with 50 mL of ethanol, and once with 50 mL of acetone by centrifuging at 4000*g* for 10 min and then left to air dry. Pre-activated yield = 480 mg.

MIL-88A(Fe) Synthesis by RAM. Iron(III) chloride hexahydrate (2.7 g, 10 mmol) and disodium fumarate (1.6 g, 10 mmol) were added to 20 mL polypropylene scintillation vials. The mixture was subjected to RAM for 60 min at accelerations of 45, 60, and 75*g*, or at a constant acceleration of 75*g* for 20 or 40 min. The dark brown product, which had formed small spheres, was transferred to a 50 mL centrifuge tube and washed twice with 50 mL of water, followed by two washes with 50 mL of acetone. Each wash step involved centrifugation at 4000*g* for 10 min. The product was then left to air dry, forming a light brown powder. Pre-activated yield = 1300 mg.

Scale Down of MIL-88A(Fe) Synthesis by RAM. For scaled down synthesis, iron(III) chloride hexahydrate (385 mg, 1.4 mmol) and disodium fumarate (228 mg, 1.4 mmol) were combined in a 1.5 mL tube and subjected to RAM 45*g* for 1 h. The product was washed twice with 1 mL water and twice with 1 mL acetone, each time by centrifuging at 10,000*g* for 5 min, then left to air dry. Pre-activated yield = 330 mg.

Scale Up of MIL-88A(Fe) Synthesis by RAM. For scaled-up synthesis, iron(III) chloride hexahydrate (13.5 g, 50 mmol) and disodium fumarate (8 g, 50 mmol) were added to a 100 mL polypropylene autoclave liner and subjected to RAM at 75*g* for 20 min. The product was then transferred to three 50 mL centrifuge tubes and washed three times with 40 mL of water, followed by three washes with 40 mL of acetone. Each wash step involved centrifugation at 4000*g* for 10 min. The product was then left to air dry. Pre-activated yield = 10.5 g.

MIL-53(Al)-FA and CaFu-1D Synthesis by RAM. For MIL-53(Al)-FA, aluminum sulfate octadecahydrate (358 mg, 0.54 mmol) and disodium fumarate (171 mg, 1.1 mmol) were combined in a 1.5 mL tube with 70 μL of 2 M sodium hydroxide and subjected to RAM for 60 min at 60*g*. The white product was washed twice in 1 mL water and twice in 1 mL ethanol by centrifuging at 10,000*g* for 5 min, then dried at room temperature under vacuum. Pre-activated yield = 114 mg. For MIL-53(Al) synthesized without NaOH, the same procedure was followed but without the addition of sodium hydroxide. Pre-activated yield = 47 mg.

The attempted synthesis of CaFu was identical except calcium acetate (251 mg 1.4 mmol) was combined with disodium fumarate (228 mg, 1.4 mmol) then washed four times with 1 mL water and twice with 1 mL ethanol. Centrifugation and drying remained the same. Pre-activated yield = 108 mg.

Estimation of Power Consumption. Power consumption of the LabRAM II was measured using a Wi-Fi-enabled smart plug (Meross, Model: MSS310) connected to a 240 V, 50 Hz

https://doi.org/10.1021/acsomega.5c02296
ACS Omega 2025, 10, 19206−19213

wall socket. Measurements were taken at idle (0g, no acceleration) and at increasing acceleration levels up to 75g with a load of 186 g (container and contents). The baseline power (74 W) was first subtracted from each measurement, and the resulting values were divided by 186 g to yield the extra power consumption per gram (ΔP in W g^{-1}) then plotted versus acceleration (Figure S10).

This was fitted with a power-law model using GraphPad Prism (v10.0.0, GraphPad Software, USA):

$$\Delta P = B_0 + B_1 \cdot a^{B_2} \quad (1)$$

where ΔP = extra power consumption per gram (W g^{-1}); a = acceleration (g or m s^{-2}). Initial parameter guesses were set as follows: $B_0 = 0$; $B_1 = 0.003$ (estimated from the average change in power per unit increase in acceleration); $B_2 = 2$ (reflecting the quadratic appearance).

After fitting, the extra power consumption was multiplied by the load mass, and the baseline (74 W) was added back to yield the total power consumption.

The power consumption for the laboratory oven was measured using the same device. During the ramp-up phase (from 17°C), the oven consumed about 109 kJ, as determined by trapezoidal integration of power readings. A short transition phase added roughly 15 kJ. In the steady-state phase, the instrument cycled between high (∼104 W) and low (∼27 W) power levels, averaging approximately 65 W. Over 4 h, this steady state accounts for roughly 933 kJ. In total, the 4 h synthesis consumed an estimated 1057 kJ.

■ ASSOCIATED CONTENT

Supporting Information

The Supporting Information is available free of charge at https://pubs.acs.org/doi/10.1021/acsomega.5c02296.

Materials and instrumentation; additional PXRD data; FTIR assignments; BET surface area data; pore size distribution; t-plot analysis; and power consumption estimation (PDF)

■ AUTHOR INFORMATION

Corresponding Author

Cara M. Doherty − *Manufacturing, CSIRO, Research Way, Clayton, Victoria 3168, Australia*; Email: Cara.Doherty@csiro.au

Authors

Laura I. FitzGerald − *Manufacturing, CSIRO, Research Way, Clayton, Victoria 3168, Australia*; orcid.org/0000-0003-2108-5173

Ashley L. Sutton − *Manufacturing, CSIRO, Research Way, Clayton, Victoria 3168, Australia*; orcid.org/0000-0002-8314-8849

Aaron J. Seeber − *Manufacturing, CSIRO, Research Way, Clayton, Victoria 3168, Australia*

Benjamin W. Muir − *Manufacturing, CSIRO, Research Way, Clayton, Victoria 3168, Australia*

Complete contact information is available at: https://pubs.acs.org/10.1021/acsomega.5c02296

Author Contributions

L.I.F. contributed to conceptualization, methodology, formal analysis, investigation, writing the original draft, and visualization. A.L.S. supported data acquisition, formal analysis, and reviewed and edited the manuscript. A.L.S. acquired, analyzed, and interpreted PXRD data. B.W.M. provided conceptual input, supervision, and resources. C.M.D. was involved in conceptualization, supervision, project administration, writing review and editing.

Notes

The authors declare no competing financial interest.

■ ACKNOWLEDGMENTS

The authors would like to thank Mark Greaves and Malisja de Vries (CSIRO Manufacturing Materials Characterization and Modelling Program) for their contributions to SEM/EDXS. In addition, we would like to thank Sam Martin (CSIRO) for the custom 3D printed Resodyn sample holder.

■ REFERENCES

(1) Zhang, Q.; Yang, H.; Zhou, T.; Chen, X.; Li, W.; Pang, H. Metal−Organic Frameworks and Their Composites for Environmental Applications. *Advanced Science* **2022**, *9*, No. 2204141.

(2) Safaei, M.; Foroughi, M. M.; Ebrahimpoor, N.; Jahani, S.; Omidi, A.; Khatami, M. A Review on Metal-Organic Frameworks: Synthesis and Applications. *TrAC - Trends in Analytical Chemistry* **2019**, *118*, 401−425.

(3) Głowniak, S.; Szczęśniak, B.; Choma, J.; Jaroniec, M. Mechanochemistry: Toward Green Synthesis of Metal−Organic Frameworks. *Mater. Today* **2021**, *46*, 109−124.

(4) Stolar, T.; Užarević, K. Mechanochemistry: An Efficient and Versatile Toolbox for Synthesis, Transformation, and Functionalization of Porous Metal-Organic Frameworks. *CrystEngComm* **2020**, *22* (27), 4511−4525.

(5) Ettlinger, R.; Lächelt, U.; Gref, R.; Horcajada, P.; Lammers, T.; Serre, C.; Couvreur, P.; Morris, R. E.; Wuttke, S. Toxicity of Metal-Organic Framework Nanoparticles: From Essential Analyses to Potential Applications. *Chem. Soc. Rev.* **2022**, *51* (2), 464−484.

(6) Bénit, P.; Letouzé, E.; Rak, M.; Aubry, L.; Burnichon, N.; Favier, J.; Gimenez-Roqueplo, A. P.; Rustin, P. Unsuspected Task for an Old Team: Succinate, Fumarate and Other Krebs Cycle Acids in Metabolic Remodeling. *Biochim Biophys Acta Bioenerg* **2014**, *1837* (8), 1330−1337.

(7) Surblé, S.; Serre, C.; Mellot-Draznieks, C.; Millange, F.; Férey, G. A New Isoreticular Class of Metal-Organic-Frameworks with the MIL-88 Topology. *Chem. Commun.* **2006**, 284−286.

(8) Leung, E.; Miller, U.; Trukhan, N.; Mattenheimer, H.; Cox, G.; Blei, S. Process for preparing porous metal-organic frameworks based on aluminum fumarate. US 2012/0082864 A1, 2012.

(9) Alvarez, E.; Guillou, N.; Martineau, C.; Bueken, B.; Van de Voorde, B.; Le Guillouzer, C.; Fabry, P.; Nouar, F.; Taulelle, F.; de Vos, D.; Chang, J.; Cho, K. H.; Ramsahye, N.; Devic, T.; Daturi, M.; Maurin, G.; Serre, C. The Structure of the Aluminum Fumarate Metal−Organic Framework A520. *Angew. Chem., Int. Ed.* **2015**, *54* (12), 3664−3668.

(10) Ke, F.; Peng, C.; Zhang, T.; Zhang, M.; Zhou, C.; Cai, H. Fumarate-Based Metal-Organic as a New Platform for highly Selective Removal of fluoride from Brick Tea. *Sci. Rep* **2018**, *8*, 939.

(11) Singh, S.; Kaushal, S.; Kaur, J.; Kaur, G.; Mittal, S. K.; Singh, P. P. CaFu MOF as an Efficient Adsorbent for Simultaneous Removal of Imidacloprid Pesticide and Cadmium Ions from Wastewater. *Chemosphere* **2021**, *272*, No. 129648.

(12) Moumen, E.; Bazzi, L.; El Hankari, S. Aluminum-Fumarate Based MOF: A Promising Environmentally Friendly Adsorbent for the Removal of Phosphate. *Process Safety and Environmental Protection* **2022**, *160*, 502−512.

(13) Viswanathan, V. P.; Mathew, S. V.; Dubal, D. P.; Adarsh, N. N.; Mathew, S. Exploring the Effect of Morphologies of Fe(III) Metal-Organic Framework MIL-88A(Fe) on the Photocatalytic Degradation of Rhodamine B. *ChemistrySelect* **2020**, *5*, 7534−7542.

(14) Fu, H.; Song, X.; Wu, L.; Zhao, C.; Wang, P.; Wang, C. Room-Temperature Preparation of MIL-88A as a Heterogeneous Photo-Fenton Catalyst for Degradation of Rhodamine B and Bisphenol a under Visible Light. *Mater. Res. Bull.* **2020**, *125*, No. 110806.
(15) Lin, K. Y. A.; Chang, H. A.; Hsu, C. J. Iron-Based Metal Organic Framework, MIL-88A, as a Heterogeneous Persulfate Catalyst for Decolorization of Rhodamine B in Water. *RSC Adv.* **2015**, *5*, 32520−32530.
(16) Ding, Y.; Ma, L.; Zeng, F.; Zhao, X.; Wang, H.; Zhu, X.; Liao, Q. Synthesis and CO2 Adsorption Kinetics of Aluminum Fumarate MOFs Pellet with High Recovery. *Energy* **2023**, *263*, No. 125723.
(17) Jeong, H.; Lee, J. 3D-Superstructured Networks Comprising Fe-MIL-88A Metal-Organic Frameworks Under Mechanochemical Conditions. *Eur. J. Inorg. Chem.* **2019**, *2019*, 4597−4600.
(18) Crawford, D.; Casaban, J.; Haydon, R.; Giri, N.; McNally, T.; James, S. L. Synthesis by Extrusion: Continuous, Large-Scale Preparation of MOFs Using Little or No Solvent. *Chem. Sci.* **2015**, *6*, 1645−1649.
(19) Titi, H. M.; Do, J.-L.; Howarth, A. J.; Nagapudi, K.; Friščić, T. Simple, Scalable Mechanosynthesis of Metal-Organic Frameworks Using Liquid-Assisted Resonant Acoustic Mixing (LA-RAM). *Chem. Sci.* **2020**, *11*, 7578−7584.
(20) Osorio, J. G.; Muzzio, F. J. Evaluation of Resonant Acoustic Mixing Performance. *Powder Technol.* **2015**, *278*, 46−56.
(21) Friščić, T.; Childs, S. L.; Rizvic, S. A. A.; Jones, W. The Role of Solvent in Mechanochemical and Sonochemical Cocrystal Formation: A Solubility-Based Approach for Predicting Cocrystallisation Outcome. *CrystEngComm* **2009**, *11*, 418−426.
(22) Afshariazar, F.; Morsali, A. The Unique Opportunities of Mechanosynthesis in Green and Scalable Fabrication of Metal-Organic Frameworks. *J. Mater. Chem. A Mater.* **2022**, *10*, 15332−15369.
(23) Raptopoulou, C. P. Metal-Organic Frameworks: Synthetic Methods and Potential Applications. *Materials* **2021**, *14* (2), 310.
(24) Sánchez-Sánchez, M.; Getachew, N.; Díaz, K.; Díaz-García, M.; Chebude, Y.; Díaz, I. Synthesis of Metal-Organic Frameworks in Water at Room Temperature: Salts as Linker Sources. *Green Chem.* **2015**, *17* (3), 1500−1509.
(25) Serre, C.; Mellot-Draznieks, C.; Surblé, N.; Audebrand, Y.; Filinchuk, G. F. Role of Solvent-Host Interactions That Lead to Very Large Swelling of Hybrid Frameworks. *Science* **2007**, *315* (5820), 1828−1831.
(26) Mellot-Draznieks, C.; Serre, C.; Surblé, S.; Audebrand, N.; Férey, G. Very Large Swelling in Hybrid Frameworks: A Combined Computational and Powder Diffraction Study. *J. Am. Chem. Soc.* **2005**, *127* (46), 16273−16278.
(27) Hadjiivanov, K. I.; Panayotov, D. A.; Mihaylov, M. Y.; Ivanova, E. Z.; Chakarova, K. K.; Andonova, S. M.; Drenchev, N. L. Power of Infrared and Raman Spectroscopies to Characterize Metal-Organic Frameworks and Investigate Their Interaction with Guest Molecules. *Chem. Rev.* **2021**, *121*, 1286−1424.
(28) Silverstein, R. M.; Webster, F. X.; Kiemle, D. J. *Spectrometric Identification of Organic Compounds*, 7th edition; Wiley, 2005.
(29) Benítez, A.; Amaro-Gahete, J.; Esquivel, D.; Romero-Salguero, F. J.; Morales, J.; Caballero, Á. MIL-88A Metal-Organic Framework as a Stable Sulfur-Host Cathode for Long-Cycle Li-S Batteries. *Nanomaterials* **2020**, *10* (3), 424.
(30) Zhao, S.; Li, Y.; Wang, M.; Chen, B.; Zhang, Y.; Sun, Y.; Chen, K.; Du, Q.; Jing, Z.; Jin, Y. Preparation of MIL-88A Micro/Nanocrystals with Different Morphologies in Different Solvents for Efficient Removal of Congo Red from Water: Synthesis, Characterization, and Adsorption Mechanisms. *Microporous and Mesoporous Materials* **2022**, *345*, No. 112241.
(31) Lázaro, I. A. A Comprehensive Thermogravimetric Analysis Multifaceted Method for the Exact Determination of the Composition of Multifunctional Metal-Organic Framework Materials. *Eur. J. Inorg. Chem.* **2020**, *2020*, 4284−4294.
(32) Wang, J.; Wan, J.; Ma, Y.; Wang, Y.; Pu, M.; Guan, Z. Metal-Organic Frameworks MIL-88A with Suitable Synthesis Conditions and Optimal Dosage for Effective Catalytic Degradation of Orange G through Persulfate Activation. *RSC Adv.* **2016**, *6*, 112502−112511.
(33) Wang, L.; Zhang, Y.; Li, X.; Xie, Y.; He, J.; Yu, J.; Song, Y. The MIL-88A-Derived Fe3O4-Carbon Hierarchical Nanocomposites for Electrochemical Sensing. *Sci. Rep* **2015**, *5*, 14341.
(34) Zhou, X.; Miao, Y.; Suslick, K. S.; Dlott, D. D. Mechanochemistry of Metal-Organic Frameworks under Pressure and Shock. *Acc. Chem. Res.* **2020**, *53*, 2806−2815.
(35) Coguill, S. L.; Martineau, Z. R. *Vessel Geometry and Fluid Properties Influencing Mix Behavior for Resonant Acoustic® Mixing Processes*; The 38th International Pyrotechnics Seminar, 2012.
(36) Gupta, M. P.; Prasad, S. M.; Sahu, R. G.; Sahu, B. N. The Crystal Structure of Calcium Fumarate Trihydrate CaC4H2O4.3-H2O. *Acta Crystallogr. B* **1972**, *28*, 135−139.
(37) Sun, S.; Henke, S.; Wharmby, M. T.; Yeung, H. H. M.; Li, W.; Cheetham, A. K. Mechanical Properties of a Calcium Dietary Supplement. *Calcium Fumarate Trihydrate. Inorg. Chem.* **2015**, *54*, 11186−11192.
(38) Cao, Z.; Jia, H.; Zhou, Y.; Li, M.; Xu, P.; Li, X.; Zheng, D. MEMS Resonant Cantilevers for High-Performance Thermogravimetric Analysis of Chemical Decomposition. *Sensors* **2023**, *23* (13), 6147.
(39) Hoffman, A. E. J.; Vanduyfhuys, L.; Nevjestić, I.; Wieme, J.; Rogge, S. M. J.; Depauw, H.; Van Der Voort, P.; Vrielinck, H.; Van Speybroeck, V. Elucidating the Vibrational Fingerprint of the Flexible Metal-Organic Framework MIL-53(Al) Using a Combined Experimental/Computational Approach. *J. Phys. Chem. C* **2018**, *122* (5), 2734−2746.
(40) Mohamadian-Kalhor, S.; Edjlali, L.; Basharnavaz, H.; Es'haghi, M. Aluminum Fumarate Metal−Organic Framework: Synthesis, Characterization, and Application as a Novel Inhibitor against Corrosion of AM60B Magnesium Alloy in Ethylene Glycol Solution. *J. Mater. Eng. Perform* **2021**, *30* (1), 720−726.
(41) Rojas-Luna, R.; Amaro-Gahete, J.; Gil-Gavilán, D. G.; Castillo-Rodríguez, M.; Jiménez-Sanchidrián, C.; Ruiz, J. R.; Esquivel, D.; Romero-Salguero, F. J. Visible-Light-Harvesting Basolite-A520 Metal Organic Framework for Photocatalytic Hydrogen Evolution. *Microporous and Mesoporous Materials* **2023**, *355*, No. 112565.
(42) Mani, M. R.; Chellaswamy, R.; Marathe, Y. N.; Pillai, V. K. Enhanced Nucleation of Polypropylene by Metal-Organic Frameworks (MOFs) Based on Aluminium Dicarboxylates: Influence of Structural Features. *RSC Adv.* **2016**, *6* (3), 1907−1912.
(43) Liu, Q.; Ding, Y.; Liao, Q.; Zhu, X.; Wang, H.; Yang, J. Fast Synthesis of Al Fumarate Metal-Organic Framework as a Novel Tetraethylenepentamine Support for Efficient CO2 Capture. *Colloids Surf., A* **2019**, *579*, No. 123645.

https://doi.org/10.1021/acsomega.5c02296
ACS Omega 2025, 10, 19206−19213